ACS APPLIED ENERGY MATERIALS

www.acsaem.org Letter

Strategic Melamine Coating on Lithium Metal for Li_3N-Rich Solid Electrolyte Interphase and Improved Battery Cycling Stability

Ju-Myung Kim, Mark H. Engelhard, Hyoju Park, Ridwan A. Ahmed, Kevin Baar, Ji-Guang Zhang, and Wu Xu*

Cite This: https://doi.org/10.1021/acsaem.6c00265 Read Online

ACCESS | Metrics & More | Article Recommendations | Supporting Information

ABSTRACT: The practical applications of lithium (Li) metal batteries (LMBs) are limited by challenges such as dendrite formation and unstable solid electrolyte interphase (SEI), especially at higher *C*-rates. This study introduces melamine-coated Li metal anodes (LMAs), forming a Li_3N-rich SEI layer that improves ionic conductivity and mechanical stability. The optimized melamine-coated LMA demonstrated uniform coverage resulting in denser Li deposition, nearly doubled cycle life (~148 cycles at 0.5 C, 1 C = 4.1 mA cm^{-2}), compared to bare Li. These findings emphasize that coating materials-induced beneficial SEI components could lead to improvement of LMB performance.

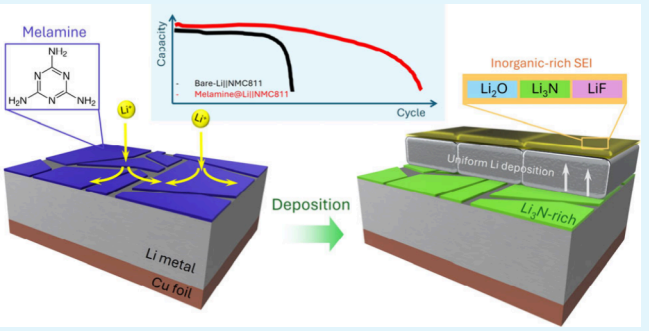

KEYWORDS: *Melamine, Li_3N, artificial solid electrolyte interphase, lithium metal, stability*

Lithium (Li) metal batteries (LMBs) are regarded as a promising high-energy-density energy storage system, due to the exceptional theoretical capacity (3860 mAh g^{-1}) and low electrochemical potential (−3.040 V vs standard hydrogen electrode) of Li metal anodes (LMAs).[1,2] However, the practical use of LMAs is hindered by intrinsic challenges, including high Li reactivity, dendrite formation, unstable solid electrolyte interphase (SEI), continuous loss of Li and electrolyte, accumulation of electrochemical inactive or "dead" Li during cycling, and subsequent short cycle life and safety risks.[3,4] To address these challenges, various protection strategies have been developed, including the application of inorganic/ceramic layers, polymeric layers, and organic/inorganic composite layers.[5,6] Most efforts have focused on stabilizing the SEI by maximizing beneficial inorganic components to enhance ionic conductivity, such as LiF (~10^{-9} S cm^{-1}),[7] Li_2O (~10^{-9} S cm^{-1}),[8] Li_3N (~10^{-3} S cm^{-1}),[9] and Li_3PO_4 (~10^{-7} S cm^{-9}).[10] Among these, Li_3N is outstanding due to its exceptional properties, which offer high ionic conductivity for efficient Li^+ migration and excellent mechanical strength.[11] Although Li_3N-rich Li protection has been previously utilized, its electrochemical performance remains limited by the low areal capacity of the cathode and the short battery lifespan.[12,13]

In this work, melamine was selected as the material for forming a Li_3N-rich SEI layer due to its nitrogen (N)-rich molecular structure, which facilitates the transformation into Li_3N on the Li metal during lithiation.[14] Melamine has previously been used as a component in three-dimensional substrates for Li-metal anodes because its abundant N-based polar groups can strongly interact with Li^+ and promote improved Li deposition.[15,16] However, these studies have not reported that melamine can contribute to Li_3N formation in the SEI layer, nor have they linked this effect to enhanced electrochemical performance. The melamine coating was applied to Li metal sheets (~50 μm) via dip coating. Three different melamine solution concentrations (0.5, 1, and 2 wt %) in dimethyl sulfoxide were tested to identify the optimized coating, with further details provided in the Experimental Method section of the Supporting Information. In this study, melamine-coated Li is referred as M*x*@Li, where "*x*" represents the weight percentage of melamine in the coating solution, i.e., *x* = 0.5, 1, and 2, respectively.

The morphologies of the Mx@Li metals are shown in Figure 1a. As the melamine content increased, the coating exhibited chunkier flakelike structures, indicating that a concentration of 2 wt % resulted in a less-uniform coverage on the LMA (Figure 1a-3), while M0.5@Li (Figure 1a-1) and M1@Li (Figure 1a-2) are displaying well-spread melamine on the surface of the LMAs. Furthermore, the Tafel curves shown in Figure S1 indicate that M0.5@Li and M1@Li have higher exchange current densities (~0.15 mA cm^{-2}) than M2@Li (~0.08 mA

Received: January 22, 2026
Revised: March 4, 2026
Accepted: March 17, 2026

https://doi.org/10.1021/acsaem.6c00265
ACS Appl. Energy Mater. XXXX, XXX, XXX−XXX

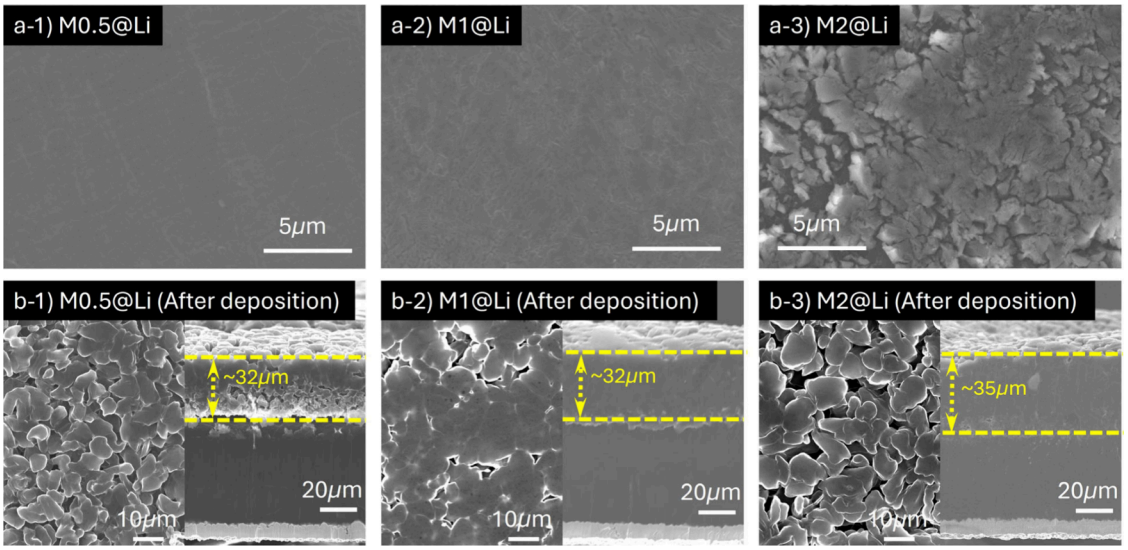

Figure 1. (a) Top-view SEM images of M*x*@Li metals. (b) Top and cross-sectional SEM images of M*x*@Li metals after the first deposition at a 0.8 mA cm^{-2} for a capacity of 4 mAh cm^{-2}.

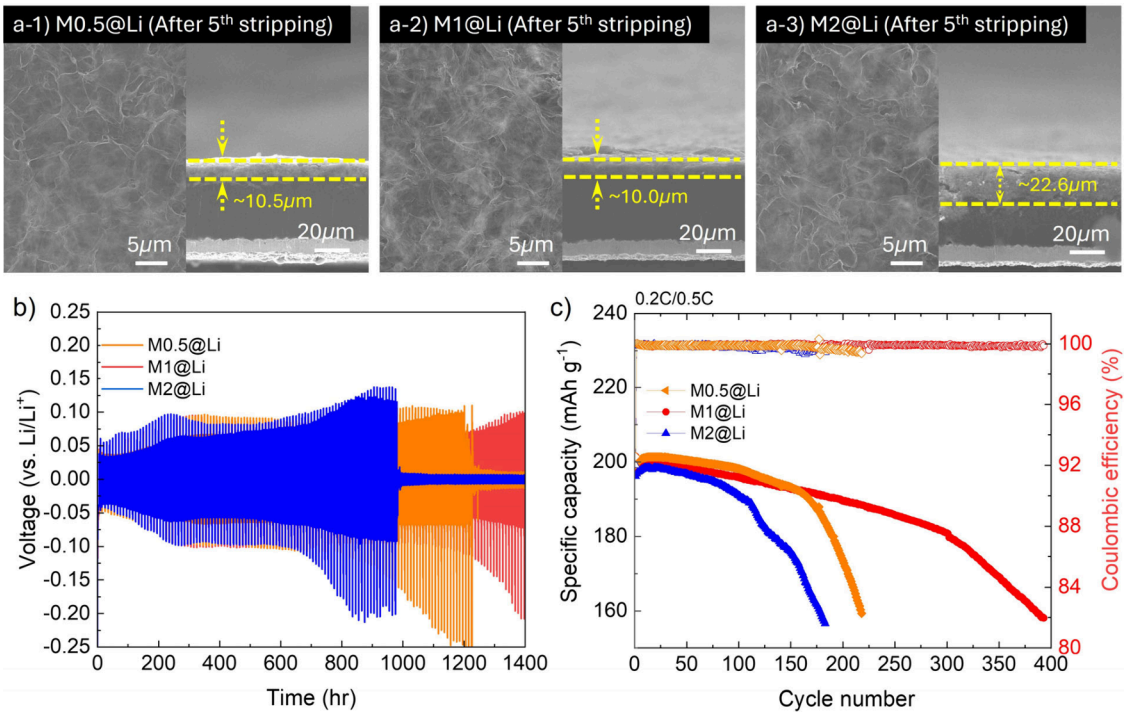

Figure 2. (a) Top and cross-sectional SEM images of M*x*@Li metals after the fifth stripping. Cycling performance of (b) Li || Li symmetric cells for a capacity of 4 mAh cm^{-2} at 0.8 mA cm^{-2} with M*x*@Li metals and (c) Li || NMC811 cells at 0.2 C charging and 0.5 C discharging.

cm^{-2}), consistent with the melamine coating morphology. These results indicate that M0.5@Li and M1@Li induce faster charge-transfer kinetics and facilitated Li^+ migration compared to M2@Li. Melamine is expected to react with Li metal to form Li_3N, promoting a uniform distribution of Li and resulting in dense Li deposition. The morphologies of deposited Li on Mx@Li metals were analyzed using scanning electron microscopy (SEM) after depositing 4 mAh cm^{-2} of Li at a current density of 0.8 mA cm^{-2} (corresponding to 0.2 C) in Li||Li symmetric cells with a localized high-concentration electrolyte consisting of LiFSI salt, 1,2-dimethoxyethane solvent and 1,1,2,2-tetrafluoroethyl-2,2,3,3-tetrafluoropropyl ether diluent at a molar ratio of 1.0:1.2:3.0. The deposition profiles are presented in Figure S2a, with a green arrow indicating the point at which the cells were disassembled for SEM imaging. As shown in Figure 1b-1, M0.5@Li exhibited a less dense surface with smaller Li particles and more pronounced porosity, compared to M1@Li (Figure 1b-2). In contrast, the cross-sectional view revealed that M1@Li displayed a denser morphology, indicating superior Li deposition behavior. M2@Li, however, showed similar particle sizes but more porous morphologies in both top and cross-sectional views with a thicker deposition (Figure 1b-3). This may result from the less uniform melamine coverage on M2@Li.

https://doi.org/10.1021/acsaem.6c00265
ACS Appl. Energy Mater. XXXX, XXX, XXX−XXX

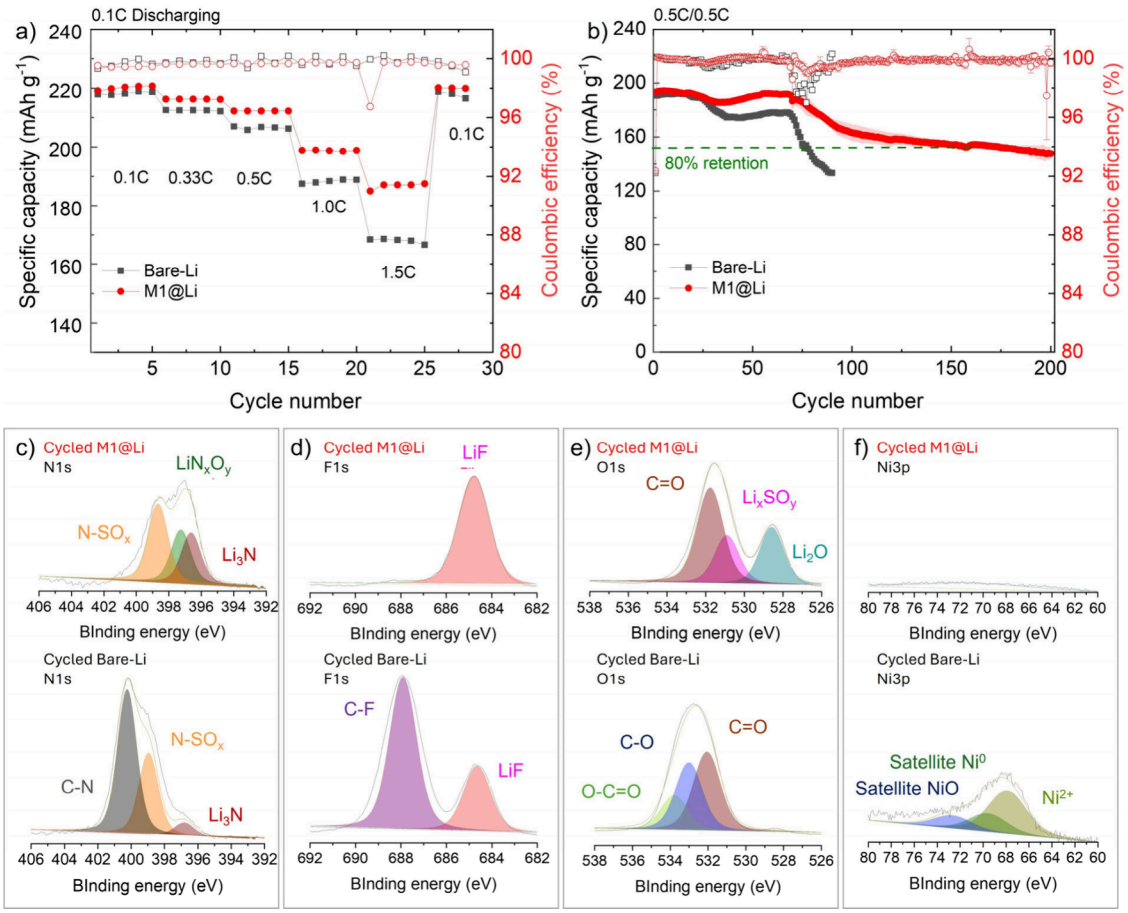

Figure 3. (a) C-rate charging capability and (b) cycling performance at 0.5 C of Li || NMC811 cells with bare Li and M1@Li. XPS (c) N 1s, (d) F 1s, (e) O 1s, and (f) Ni 3p spectra of cycled LMAs in Li || NMC811 cells at 0.5 C (bare Li: after 90 cycles, M1@Li: after 148 cycles).

To evaluate the influence of Mx@Li metals on electrochemical performance during repeated Li deposition and stripping, Li||Li symmetric tests were conducted, with Li deposited/stripped at a current density of 0.8 mA cm^{-2} and a capacity of 4 mAh cm^{-2} using the three Mx@Li metals. After the first cycle, M2@Li exhibited higher overpotentials compared to the other two samples. To gain a deeper understanding, the top and cross-sectional views of Mx@Li metals after the fifth stripping cycle (marked by a purple arrow in Figure S2a) were analyzed using SEM (Figure 2a). While the top-view images of M*x*@Li metals showed no significant differences, M0.5@Li (Figure 2a-1) and M1@Li (Figure 2a-2) displayed thinner accumulated SEI layers while preserving a thicker fresh Li layer. In comparison, M2@Li exhibited a thicker accumulated SEI layer (Figure 2a-3), indicative of increased side reactions that contributed to its higher overpotential. Moreover, M2@Li and M0.5@Li failed after 980 and 1230 h, respectively (Figure S2b and S2c). In contrast, M1@Li maintained lower overpotentials than others, sustaining up to 1400 h of cycling (Figure 2b and Figure S2d). These results correlate with the morphological features of Li after deposition and stripping, as discussed in Figure 1b and Figure 2a.

Li || $LiNi_{0.8}Mn_{0.1}Co_{0.1}O_2$ (NMC811) cells with the M*x*@Li metals were evaluated under a voltage range of 2.8−4.4 V, with charge/discharge rates of 0.2 C and 0.5 C, respectively, following two formation cycles at 0.1 C (where 1 C = 4.1 mAh cm^{-2}). During the initial formation cycles, all M*x*@Li-based cells delivered a similar first discharge capacity of 210.5 mAh g^{-1} (Figure S3). However, at the first cycle of 0.2 C/0.5 C, M0.5@Li exhibited a slightly higher discharge capacity (199.2 mAh g^{-1}) compared to M1@Li (197.6 mAh g^{-1}) and M2@Li (196.1 mAh g^{-1}) (Figure 2b). All cells were tested until reaching 80% capacity retention, wherein M1@Li demonstrated superior battery life by extending up to the 393rd cycle, outperforming M0.5@Li (~218th cycle) and M2@Li (~182nd cycle). Based on these results, M1@Li was identified as the optimized Mx@Li for comparison with bare Li.

The Li deposition morphology of Bare-Li was analyzed under the same conditions as shown in Figure 1b. From the top-view SEM images (Figure S4a), Bare-Li exhibited a more porous structure compared to the denser morphology observed for M1@Li (Figure 1b-2). Additionally, cross-sectional SEM images revealed that deposited Li on Bare-Li in Bare-Li||Bare-Li cells was less compact than on M1@Li in M1@Li||M1@Li. Moreover, after the fifth stripping, Bare-Li exhibited a thicker accumulated SEI layer (~21.1 μmm (Figure S4b) compared to M1@Li (~10.0 μm) (Figure 2a-2). This structural disparity was reflected in the performance of Li || Li symmetric cells, where bare Li achieved a shorter cycle life (~1300 h, Figure S4c) compared to M1@Li that showed stable performance up to 1400 h (Figure 2b). Furthermore, Li || NMC811 cells with bare Li under the same conditions as those in Figure 2c delivered a shorter life (80% of capacity retention after the 275th cycle) (Figure S4d) than M1@Li||NMC811 cells. Based on these results, it can be inferred that M*x*@Li may

https://doi.org/10.1021/acsaem.6c00265
ACS Appl. Energy Mater. XXXX, XXX, XXX−XXX

Scheme 1. Illustration of the Advantages of Melamine-Coated LMA

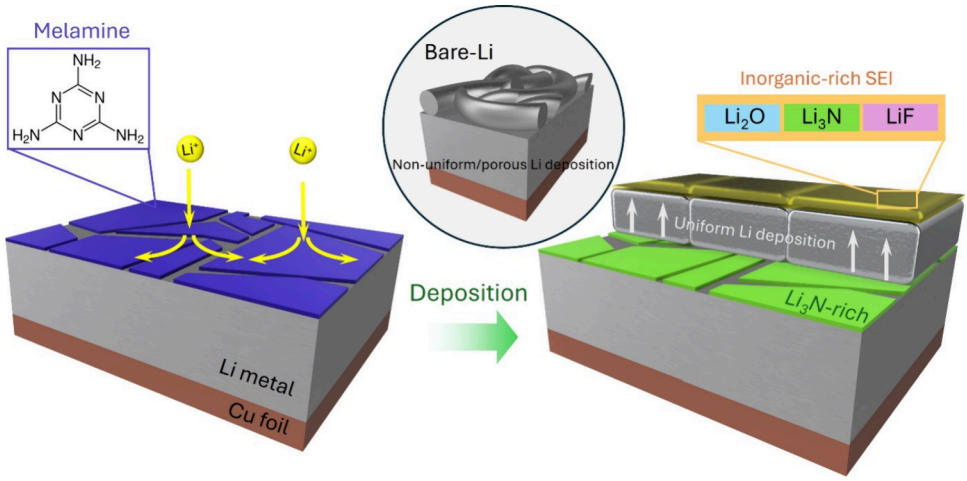

outperform bare Li in Li||NMC811 cells under even harsher conditions as well.

Since stable Li deposition becomes more challenging at higher current densities,[17,18] improved Li deposition can facilitate better high C-rate charging performance. Li || NMC811 cells with bare Li and M1@Li were discharged at 0.1 C (1 C = 4.1 mA cm^{-2}) and charged at varying rates from 0.1 C to 1.5 C after two formation cycles at 0.1 C within a voltage range of 2.8−4.4 V (vs Li/Li^+). M1@Li||NMC811 cells consistently delivered higher capacities at various charging current densities compared to cells with bare Li (Figure 3a). Notably, the cell with M1@Li achieved increased discharge capacities even at a high charge rate of 1.5 C (187.1 mAh g^{-1}), compared to bare Li (168.3 mAh g^{-1}). Unlike the voltage profiles at 0.1 C charging, which do not show distinguishable differences, bare Li || NMC811 cells displayed significantly higher overpotential during charging at 1.5 C compared to M1@Li || NMC811 (Figure S5). This suggests that the melamine coating played a role in enhancing performance. Furthermore, the cyclability of Li || NMC811 cells with bare Li and M1@Li was evaluated at a charge/discharge rate of 0.5 C (Figure 3b). The M1@Li || NMC811 cell retained 80% of its initial capacity (193.4 mAh g^{-1}) after 148 cycles, whereas bare-Li || NMC811 reached 80% capacity retention after only 78 cycles, starting from an initial capacity of 190.6 mAh g^{-1}. M1@Li demonstrated both a higher initial capacity and an extended battery life at higher current densities (over 2 mA cm^{-2}). Also, M1@Li exhibited a lower SEI resistance (~5.1 Ω) than bare Li (~6.6 Ω) after the first formation cycle, indicating that the Li_3N formed by melamine reduced the interfacial resistance (Figure S6). These results underline that melamine coating on Li metal significantly enhances the interphase on the LMA during cycling, thereby improving overall battery performance.

X-ray photoelectron spectroscopy (XPS) was conducted to investigate LMAs of Li || NMC811 cells after 148 cycles with M1@Li and 90 cycles with bare Li. As shown in Figure 3c, the N 1s spectra for both cycled LMAs revealed decomposition products, such as N−S species, resulting from the breakdown of the LiFSI salt in the electrolyte.[19] Remarkably, the cycled M1@Li exhibited a stronger Li_3N peak (N 1s, 396.8 eV)[20] compared to the cycled bare Li, confirming that melamine promotes the formation of a Li_3N-enriched SEI layer on Mx@Li as expected. The melamine coating formed a flakelike structure on the surface of LMAs (Figure S7a), suggesting that most Li ions were deposited on the LMA surface, reacting with melamine. Additionally, the XPS N 1s spectra of the fresh M1@Li disclosed melamine peaks (−NH_2 and C═N)[21] without Li_3N (Figure S7b), indicating that Li was deposited onto the coating layer and subsequently reacted with it. Besides, the cycled M1@Li showed more inorganic components (LiN_xO_y)[22] while the cycled bare Li presented organic species (C−N). As Li_3N is recognized as a beneficial inorganic component that facilitates rapid Li ion transfer across the interphase and enhances ionic conductivity of the SEI layer, these findings explain the improved cycling performance of M1@Li compared to bare Li in Li || NMC811 cells at 0.5 C (Figure 3c). In the next step, depth-profiling analyses will be performed to gain a more detailed understanding of the melamine-induced SEI chemistry and interphase stability on Li metal.

Furthermore, the F 1s spectra (Figure 3d) disclosed a weaker LiF peak and a C−F peak associated with organic components in the cycled bare Li. However, the cycled M1@Li displayed a dominant LiF peak (F 1s, 684.7 eV),[23] suggesting that the melamine-induced Li_3N contributed to enhanced Li-ion migration during cycling. Moreover, the O 1s spectra of cycled M1@Li revealed an inorganic-dominant SEI composition, including Li_2O (O 1s, 528.5 eV),[24] which contributes to improved mechanical stability (Figure 3e). In contrast, the cycled bare Li predominantly displayed organic components. The stabilized interphase on LMAs seems to have positively impacted the NMC811 cathode, as an unstable SEI layer can dissolve into the electrolyte, leading to its degradation. Dissolved species and decomposed electrolytes from the anode may move to the cathode, disrupting Li ion transport and overall battery performance. This inverse cross-talk from the anode to the cathode can lead to severe cathode degradation and further exacerbate cross-talk.[25−27] Cycled bare Li showed Ni species on the surface (Figure 3f),[28] indicating that dissolved Ni ions had moved from the NMC811 cathode due to structural degradation. However, the cycled M1@Li exhibited no discernible Ni species peaks, confirming its improved stability. To further investigate the impact of cross-talk on the NMC811 cathode, X-ray diffraction (XRD) was performed after cycling (Figure S8a). The phase transformation from a layered structure to a rock-salt structure occurs due to cation mixing between Li ions and Ni ions, which share a similar ionic radius. This cation mixing layer

https://doi.org/10.1021/acsaem.6c00265
ACS Appl. Energy Mater. XXXX, XXX, XXX−XXX

hinders Li-ion migration, resulting in poor cycling performance. A lower $I(003)/I(104)$ peak intensity ratio reflects a greater degree of cation mixing, which is related to structural degradation.[29,30] NMC811 paired with M1@Li (2.06) retained the layered structure more effectively compared to NMC811 paired with bare Li (1.12). Additionally, the SEM image of cycled NMC811 paired with M1@Li showed no visible cracks on the surface (Figure S8b). In contrast, cycled NMC811 paired with bare Li exhibited evident cracks (Figure S8c), suggesting that it experienced more severe reverse cross-talk. Remarkably, the cycling performance of M1@Li‖NMC811 surpasses the previously reported inorganic material-coated Li metal, even at higher areal capacities and *C*-rates (Table S1). The beneficial impact of the melamine coating on LMAs is illustrated in Scheme 1.

In summary, this study demonstrates the effectiveness of melamine-coated LMAs in improving the performance of LMBs. The optimized melamine-coated LMA (M1@Li) achieved uniform coverage and facilitated the formation of a Li_3N-rich SEI layer, contributing to enhanced ionic conductivity, mechanical stability, and reduced interphase side reactions. Compared to bare Li, M1@Li exhibited significantly improved cycle life, boosted high C-rate performance, and stabilized interphase, as evidenced by denser Li deposition, reduced overpotentials, and dominant inorganic SEI components such as Li_3N, Li_2O, and LiF. The stabilized SEI also contributed to alleviating cathode degradation by preventing side reactions on the cathode via cross-talk. These findings establish the way of using melamine-induced SEI components as a promising strategy to enhance the longevity and functionality of LMBs, particularly under demanding cycling conditions.

■ ASSOCIATED CONTENT

Supporting Information

The Supporting Information is available free of charge at https://pubs.acs.org/doi/10.1021/acsaem.6c00265.

Experimental section, additional electrochemical data, characterization data, and comparison table (PDF)

■ AUTHOR INFORMATION

Corresponding Author

Wu Xu − *Energy and Environment Directorate, Pacific Northwest National Laboratory, Richland, Washington 99354, United States;* orcid.org/0000-0002-2685-8684; Email: wu.xu@pnnl.gov

Authors

Ju-Myung Kim − *Energy and Environment Directorate, Pacific Northwest National Laboratory, Richland, Washington 99354, United States;* orcid.org/0000-0003-0851-1959

Mark H. Engelhard − *Energy and Environment Directorate, Pacific Northwest National Laboratory, Richland, Washington 99354, United States;* orcid.org/0000-0002-5543-0812

Hyoju Park − *Physical and Computational Sciences Directorate, Pacific Northwest National Laboratory, Richland, Washington 99354, United States*

Ridwan A. Ahmed − *Energy and Environment Directorate, Pacific Northwest National Laboratory, Richland, Washington 99354, United States*

Kevin Baar − *Energy and Environment Directorate, Pacific Northwest National Laboratory, Richland, Washington 99354, United States*

Ji-Guang Zhang − *Energy and Environment Directorate, Pacific Northwest National Laboratory, Richland, Washington 99354, United States;* orcid.org/0000-0001-7343-4609

Complete contact information is available at: https://pubs.acs.org/10.1021/acsaem.6c00265

Author Contributions

Ju-Myung Kim: Conceptualization, Methodology, Formal analysis, Data curation, Writing−Original draft. **Mark H. Engelhard, Hyoju Park, Ridwan A. Ahmed, Kevin T. Baar, Ji-Guang Zhang:** Methodology, Data curation, Writing−Review and editing. **Wu Xu:** Conceptualization, Funding acquisition, Project administration, Writing−Review and editing.

Notes

The authors declare no competing financial interest.

■ ACKNOWLEDGMENTS

This work was supported by the Assistant Secretary for Energy Efficiency and Renewable Energy, Vehicle Technologies Office of the U.S. Department of Energy (DOE) through the Advanced Battery Materials Research (BMR) program, under Contract No. DE-AC05-76RL01830 for Pacific Northwest National Laboratory (PNNL). Battery500 Consortium is acknowledged for supplying the NMC811 laminates. The microscopic and spectroscopic characterizations were conducted in the William R. Wiley Environmental Molecular Sciences Laboratory (EMSL), a national scientific user facility sponsored by DOE's Office of Biological and Environmental Research and located at PNNL. Part of the electron microscopy work is carried out by using instruments that are funded in part by a grant from the Washington State Department of Commerce's Clean Energy Fund. PNNL is operated by Battelle for the DOE, under Contract DE-AC05-76RL01830. The salt LiFSI was provided by Dr. Kazuhiko Murata of Nippon Shokubai Co., Ltd.

■ REFERENCES

(1) Zhang, X.; Yang, Y.; Zhou, Z. Towards practical lithium-metal anodes. *Chem. Soc. Rev.* **2020**, *49* (10), 3040−3071.

(2) Jie, Y.; Tang, C.; Xu, Y.; Guo, Y.; Li, W.; Chen, Y.; Jia, H.; Zhang, J.; Yang, M.; Cao, R.; et al. Progress and perspectives on the development of pouch-type lithium metal batteries. *Angew. Chem.* **2024**, *136* (7), No. e202307802.

(3) Liu, D.-H.; Bai, Z.; Li, M.; Yu, A.; Luo, D.; Liu, W.; Yang, L.; Lu, J.; Amine, K.; Chen, Z. Developing high safety Li-metal anodes for future high-energy Li-metal batteries: strategies and perspectives. *Chem. Soc. Rev.* **2020**, *49* (15), 5407−5445.

(4) Zhang, J.-G.; Xu, W.; Xiao, J.; Cao, X.; Liu, J. Lithium metal anodes with nonaqueous electrolytes. *Chem. Rev.* **2020**, *120* (24), 13312−13348.

(5) Li, J.; Kong, Z.; Liu, X.; Zheng, B.; Fan, Q. H.; Garratt, E.; Schuelke, T.; Wang, K.; Xu, H.; Jin, H. Strategies to anode protection in lithium metal battery: A review. *InfoMat* **2021**, *3* (12), 1333−1363.

(6) Han, Z.; Zhang, C.; Lin, Q.; Zhang, Y.; Deng, Y.; Han, J.; Wu, D.; Kang, F.; Yang, Q. H.; Lv, W. A protective layer for lithium metal anode: why and how. *Small Methods* **2021**, *5* (4), No. 2001035.

(7) He, M.; Guo, R.; Hobold, G. M.; Gao, H.; Gallant, B. M. The intrinsic behavior of lithium fluoride in solid electrolyte interphases on lithium. *Proc. Natl. U. S. A.* **2020**, *117* (1), 73−79.
(8) Lorger, S.; Usiskin, R.; Maier, J. Transport and charge carrier chemistry in lithium oxide. *J. Electrochem. Soc.* **2019**, *166* (10), A2215−A2220.
(9) Ren, P.; Wang, X.; Huang, B.; Liu, Z.; Liu, R. Li3N interlayer enables stable long-term cycling for sulfide-based all-solid-state Li metal batteries. *J. Energy Storage* **2024**, *82*, No. 110200.
(10) Wang, L.; Wang, Q.; Jia, W.; Chen, S.; Gao, P.; Li, J. Li metal coated with amorphous Li3PO4 via magnetron sputtering for stable and long-cycle life lithium metal batteries. *J. Power Sources* **2017**, *342*, 175−182.
(11) Wang, Z.; Wang, Y.; Wu, C.; Pang, W. K.; Mao, J.; Guo, Z. Constructing nitrided interfaces for stabilizing Li metal electrodes in liquid electrolytes. *Chem. Sci.* **2021**, *12* (26), 8945−8966.
(12) Kim, S.; Kim, T.; Oh, W.; Kim, J.; Lee, C.; Jo, W.; Choi, J.; Lee, D.; Sun, S. Lithium Nitride-rich Li Protection Layer via Facile Lewis Acid−Base Reaction for Li Metal Batteries. *Ind. Eng. Chem. Res.* **2025**, *64* (40), 19322−19331.
(13) Huang, X.; Zhou, H.; Li, Z.; Geng, T.; Si, Y.; Fang, Z.; Xu, Z.; Zhang, S.; Feng, T.; Wu, M. Plasma-Induced LiF/Li3N Hybrid Interphase: A Scalable Strategy for Ultrastable Lithium Metal Anodes at High Current Densities. *ACS Appl. Energy Mater.* **2025**, *8* (24), 17900−17909.
(14) Cai, J.-X.; Zhu, H.-L.; Liu, W.; Qi, Y.-X.; Yang, H.; Li, T.; Bai, Y.-J. Constructing melamine coating convertible into solid electrolytes to enhance the electrochemical performance of Li2ZnTi3O8 anode. *Mater. Today Sustain.* **2022**, *19*, No. 100192.
(15) Xiang, S.-B.; Zhang, X.; Hou, Y.; Li, W.; Yin, C.; Yin, Z. 3D soft lithiophilic current collector of Ag-CuNW/MWCNT@ melamine foam enables dendrite-free lithium metal anodes. *J. Mater. Chem. A* **2024**, *12* (44), 30601−30610.
(16) Fan, L.; Zhuang, H. L.; Zhang, W.; Fu, Y.; Liao, Z.; Lu, Y. Stable lithium electrodeposition at ultra-high current densities enabled by 3D PMF/Li composite anode. *Adv. Energy Mater.* **2018**, *8* (15), No. 1703360.
(17) Kim, S.; Park, G.; Lee, S. J.; Seo, S.; Ryu, K.; Kim, C. H.; Choi, J. W. Lithium-metal batteries: from fundamental research to industrialization. *Adv. Mater.* **2023**, *35* (43), No. 2206625.
(18) Kim, J. M.; Engelhard, M. H.; Lu, B.; Xu, Y.; Tan, S.; Matthews, B. E.; Tripathi, S.; Cao, X.; Niu, C.; Hu, E.; et al. High current-density-charging lithium metal batteries enabled by double-layer protected lithium metal anode. *Adv. Funct. Mater.* **2022**, *32* (48), No. 2207172.
(19) Li, Y.; Liu, M.; Wang, K.; Li, C.; Lu, Y.; Choudhary, A.; Ottley, T.; Bedrov, D.; Xing, L.; Li, W. Single-Solvent-Based Electrolyte Enabling a High-Voltage Lithium-Metal Battery with Long Cycle Life. *Adv. Energy Mater.* **2023**, *13* (30), No. 2300918.
(20) Li, T.; Li, Y.; Sun, Y.; Qian, Z.; Wang, R. New insights on the good compatibility of ether-based localized high-concentration electrolyte with lithium metal. *ACS Mater. Lett.* **2021**, *3* (6), 838−844.
(21) Dementjev, A.; De Graaf, A.; Van de Sanden, M.; Maslakov, K.; Naumkin, A.; Serov, A. X-Ray photoelectron spectroscopy reference data for identification of the C3N4 phase in carbon−nitrogen films. *Diamond Relat. Mater.* **2000**, *9* (11), 1904−1907.
(22) Sun, Z.; Tan, Y.; Zhan, Y.; Li, K.; Dou, W.; Wang, C.; Lin, X.; Yuan, R.; Yan, J.; Zheng, M.; Dong, Q. An Organic Redox Mediator with a Defense-Donor for Lithium Anode in Lithium−Oxygen Batteries. *Small Methods* **2023**, *7* (2), No. 2201289.
(23) Gao, J.; Gong, B.; Zhang, Q.; Wang, G.; Dai, Y.; Fan, W. Study of the surface reaction mechanism of Li4Ti5O12 anode for lithium-ion cells. *Ionics* **2015**, *21* (9), 2409−2416.
(24) Qin, N.; Jin, L.; Lu, Y.; Wu, Q.; Zheng, J.; Zhang, C.; Chen, Z.; Zheng, J. P. Over-potential tailored thin and dense lithium carbonate growth in solid electrolyte interphase for advanced lithium ion batteries. *Adv. Energy Mater.* **2022**, *12* (15), No. 2103402.
(25) Arifiadi, A.; Demelash, F.; Abke, N. M.; Brake, T.; Vahnstiege, M.; Alsheimer, L.; Wiemers-Meyer, S.; Winter, M.; Kasnatscheew, J. Assessment of "Inverse" Cross-Talk (Anode to Cathode) in High-Voltage Li/Mn-Rich Layered Oxide‖ Li Cells. *Adv. Funct. Mater.* **2025**, *35* (7), No. 2413958.
(26) Björklund, E.; Brandell, D.; Hahlin, M.; Edström, K.; Younesi, R. How the negative electrode influences interfacial and electrochemical properties of $LiNi_{1/3}Co_{1/3}Mn_{1/3O}2$ cathodes in Li-ion batteries. *J. Electrochem. Soc.* **2017**, *164* (13), No. A3054.
(27) Lee, H.; Lim, H.-S.; Ren, X.; Yu, L.; Engelhard, M. H.; Han, K. S.; Lee, J.; Kim, H.-T.; Xiao, J.; Liu, J.; Xu, W.; Zhang, J.-G. Detrimental effects of chemical crossover from the lithium anode to cathode in rechargeable lithium metal batteries. *ACS Energy Lett.* **2018**, *3* (12), 2921−2930.
(28) Tarditi, A. M.; Barroso, N.; Galetti, A. E.; Arrúa, L. A.; Cornaglia, L.; Abello, M. C. XPS study of the surface properties and Ni particle size determination of Ni-supported catalysts. *Surf. Interface Anal.* **2014**, *46* (8), 521−529.
(29) Sim, S.-J.; Lee, S.-H.; Jin, B.-S.; Kim, H.-S. Use of carbon coating on LiNi0. 8Co0. 1Mn0. 1O2 cathode material for enhanced performances of lithium-ion batteries. *Sci. Rep.* **2020**, *10* (1), No. 11114.
(30) Jiang, M.; Danilov, D. L.; Eichel, R. A.; Notten, P. H. A review of degradation mechanisms and recent achievements for Ni-rich cathode-based Li-ion batteries. *Adv. Energy Mater.* **2021**, *11* (48), No. 2103005.

https://doi.org/10.1021/acsaem.6c00265
ACS Appl. Energy Mater. XXXX, XXX, XXX−XXX